Computer Physics Communications 183 (2012) 2089–2097

Contents lists available at SciVerse ScienceDirect

Computer Physics Communications

journal homepage: www.elsevier.com/locate/cpc

An efficient model for studying the dynamics of frustrated systems

Alejandro León

Facultad de Ingeniería, Universidad Diego Portales, Santiago, Chile

ARTICLE INFO

Article history:
Received 3 February 2012
Received in revised form
9 May 2012
Accepted 9 May 2012
Available online 19 May 2012

Keywords:
Magnetic monopoles
Frustrated systems
Cellular automata
Spin ice

ABSTRACT

We present a model based on determinist cellular automata architecture for studying systems with frustrated interactions that present elemental excitations, such as magnetic monopoles. This model is especially designed to be applied for systems with components that have energy levels much higher than kT. This would imply that for these systems thermal fluctuations are negligible and they can be analyzed under the supposition that the dynamic is produced at zero temperature. This category includes artificial magnetic spin ice systems and donor and recipient electrical charge molecular systems. The dynamics of these systems can be simulated in real time with this model, with a minimum of computational requirements. It can be an excellent complement to Monte Carlo methods and in some cases can even replace them directly. In this report, we show the designed structure and some interesting results obtained in studying the dynamics of emergent magnetic monopoles in artificial spin ice systems and excitations in graphane molecular arrays.

Introduction

Artificial spin ice systems

Frustrated physical systems have interactions that cannot be simultaneously minimized. A consequence of this frustration is that these systems present residual entropy at zero temperature. Water ice is one of the most often cited examples of this type of system [1]. Natural spin ice systems in rare earths have recently received much attention from researchers because elemental excitations equivalent to magnetic monopoles have been detected at sub-kelvin temperatures [2–4]. Artificial spin ice systems are arrays of nanomagnets with anisotropy energy on the order of 10^4 K [5]. This allows their study at ambient temperature and the simulation of the behavior of natural spin ice systems [6,7]. A recent report of Mengotti [8] reported the first direct observation of emergent magnetic monopoles in artificial spin ice systems. All these experimental results have provided considerable information about these frustrated systems, but at the same time have raised many unanswered questions about some situations on which experiments have not shed any light. Because of this, it is necessary to have robust models for simulating the complex dynamics of these elemental excitations.

Frustrated molecular systems

In many problems at the molecular level, electrical interaction cannot be minimized completely owing to frustration. In particular, there is a proposal to propagate and process digital information using the polarization of a molecular array [9,10]. In the logic gates defined for this technological proposal, the phenomenon of frustration is presented in the minimization of electrostatic energy. To correctly assess the performance of these and similar systems, simple models are needed to simulate the dynamics of electrical charges in these systems.

Cellular automata (CA)

Cellular automata are models used to simulate the dynamics of complex systems. The main idea is to define an array of entities (cells of the automaton) that have a discrete set of states. The change of state of a particular cell is defined with updating rules for the automaton and depends on the state of the cells being considered and the state of neighboring cells. A variety of models based on CA have been used to efficiently study problems in biology, physics, chemistry, engineering and materials sciences [11,12]. They represent an excellent alternative to models based on differential equations and to Monte Carlo algorithms because they can simulate highly complex systems with a low computational cost. The first attempt to use CA in the study of magnetism was that with the model proposed by Vichniac [13], which was subsequently developed by Pomeau [14] and Hermann [15] and is termed the VPH model. This is being used to resolve an Ising type spin system. To avoid a "feedback catastrophe", the automaton is updated in more than one step. The model functions well at high temperatures ($T > T_C$), but fails at low temperatures. Subsequently, Ottavi et al. [16] used a microcanonical algorithm in a CA to resolve the Ising spin system. A determinist version of this model provided acceptable results at a low temperature [16]. A more recent model studies the Ising model

E-mail address: alejandro.leon@udp.cl.

0010-4655/$ – see front matter © 2012 Elsevier B.V. All rights reserved.
doi:10.1016/j.cpc.2012.05.011

using a quantum algorithm in a cellular automaton [17]. The 2D simulation shows a good agreement with the analytical solution. Our work shows the design of a model based on the architecture of a cellular automaton for the study of frustrated magnetic and electrical systems.

Frustrated cellular automata (FCA)

Our model consists of a cellular automaton composed of cells that are connected at n first neighbors. The number n will be called the coordination number. Fig. 1 shows three examples where we can apply the FCA model. Fig. 1(a) shows a squared network with $n = 4$. The cells of the automaton are represented by red and yellow circles. We can see in the figure that each cell is connected at four first neighbors, such that each red cell is connected at four yellow cells and each yellow cell is connected at four red cells. For this squared geometry, we have four connections (north, west, south and east). The "eastern" connection of the yellow cell is the "western" connection of the red cell. With this color code, we can define four connections that surround each cell. Horizontally, we have the "yellow–red" connections and the "red–yellow" connections". Analogous to this, vertically, we have the same "red–yellow" and "yellow–red" connections. By way of examples, Fig. 1(a) shows the horizontal "yellow–red" connections. Fig. 1(b) shows a hexagonal network as red and yellow circles with $n = 3$. Each red cell is connected to three yellow cells and vice versa, and Fig. 1(b) shows the horizontal connections. A one-dimensional FCA is represented by the horizontal lines in Fig. 1(c) with $n = 2$ (in this case there are two kinds of connections). The updating function $u(t)$ is defined in n steps, updating the n nodes for each cell, as indicated in expression (1):

$$u_1(t) \rightarrow u_2(t) \dashrightarrow u_n(t) \Rightarrow u(t). \tag{1}$$

In this expression, u_1 represents the updating of connector 1, u_2 represents the updating of connector 2, etc. Once the updating of the connections is completed, the entire FCA has been updated.

Because the structure of the FCA model is completely general, the form of the function of partial u_k updating depends on the physical nature of the phenomenon that is being modeled. However, the FCA automaton was designed to study systems composed of magnetic nanoislands and polar molecular systems with anisotropy energy much greater than kT. This implies that the thermal fluctuations are negligible and they can be considered as systems with temperatures equivalent to 0 K. For magnetic systems, the connections correspond to magnetic nanoislands. For molecular systems, the connections correspond to the direction of the electrical dipolar moment. In both cases, the partial u_k updating corresponds to reversing the magnetic or electrical moment. A very important objective for the study of these systems is to learn about the elemental excitations that are generated by the collaboration of many of these entities (emergent magnetic monopoles, for example). Given this, the energy of the system was assessed in the framework of magnetic or electrical charges.

General conditions to be met by systems that are simulated with the FCA:

- The system must have a regular array of elementary entities (magnets or molecules).
- The energy barrier for reversal (or tunneling energy for the molecular case) must be much greater than the energy at room temperature.

The FCA algorithm

Having defined the structure of the FCA, we will now explain the global functioning of the proposed architecture.

Step 1: A connection is chosen randomly, among the available n.

Step 2: The automaton is reviewed in each cell and the chosen connection at point 1 is updated (reversing the magnetic moment or electric moment).

If $\Delta E \leq -E_{\text{Anisotropy}}$, the change is accepted (magnetic case). If $\Delta E \leq E_{\text{Tunneling}}$, the change is accepted (molecular case).

Step 3: A connection is randomly chosen from among the $n - 1$ and step 2 is repeated.

Step 4: Once the connections are completed, the global updating of the FCA is completed. At this stage, the physical observables of the system (polarization, density of the charges, Dirac string, etc.) are assessed.

Step 1 is repeated.

The description of the FCA algorithm has been proposed in general terms, but we can incorporate variants in step 1. Instead of making the choice randomly, we can define a particular sequence for making the partial u_k updating, and maintain this sequence for all the steps of the algorithm. For example, for the square lattice we work with the sequence $u_1 \rightarrow u_2 \rightarrow u_3 \rightarrow u_4$. Another possible variation in step 1 of the FCA algorithm is to choose combinations of connections in the network. For example, in the hexagonal network we can choose the sequence $[(u_1 \vee u_2) \rightarrow u_3](t) \rightarrow [(u_1 \vee u_2) \rightarrow u_3](t+1)$. This sequence means choosing between connectors 1 and 2, updating the chosen connector and then updating connector 3. In the following global step of the algorithm we return to choosing between connectors 1 and 2, and the chosen connector is updated and then connector 3 is updated. These variants are not strictly necessary in the algorithm and are only used to efficiently study some observable in particular, as will be explained further on in the applications.

Applications of the FCA

Emergent magnetic monopoles in the hexagonal network

To illustrate the behavior of the model, we begin by studying the hexagonal network. The parameters used in this study correspond to those of the experimental work of Mengotti et al. [6]. We study the density of emergent monopoles in a global sequence of magnetic reversal.

The system studied in this work is a magnetic nanoisland array in a hexagonal lattice. Fig. 2(a) shows a scheme of the magnetic bars arranged on the sides of a hexagon and Fig. 2(b) shows the frustration in the hexagonal network. Three nanomagnets converge in the vertices of the hexagons, as can be appreciated in Fig. 2. Topologically, we can define two non-equivalent vertices in the hexagonal lattice, vertices A and B. The two non-equivalent vertices form the unit cell of the entire array. The cell is shown in red in Fig. 2(a). In the magnetic charge model, the charges are concentrated in these vertices. We define the magnetic charge at a vertex as -1, when two south poles and a north pole, of the three nanomagnets that form the vertex, converge. Equally, we define the magnetic charge as $+1$, when two north poles and a south pole converge in the vertex considered. Fig. 3 shows the array with an applied magnetic field. The upper left of Fig. 3 shows the array subjected to a field in the direction of the negative axis x. In the lower left of the figure the field is shown directed to the right. The nanomagnets with the x component of the magnetic moment directed to the left are represented by gray bars, and the nanomagnets with the x component from the magnetic moment directed to the right are represented by black bars. When the sample is totally magnetized in directions $+x$ or $-x$, all the type A vertices have $+1$ or -1 charges, while all the B vertices have -1 or $+1$ charges. This can be seen in Fig. 3.

We suppose that we are under the condition of total magnetization, with the magnetic field directed to the left (upper left

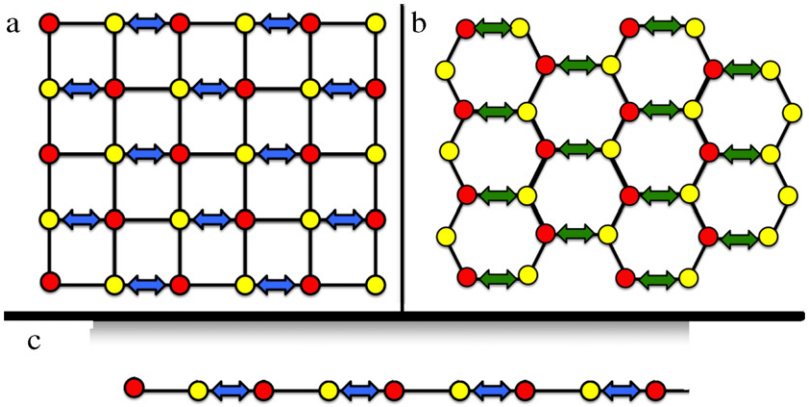

Fig. 1. (a) Square network with $n = 4$. The figure shows one of the four possible interactions that are updated (with the double blue arrow). We can see in the figure that for a yellow node the interaction is with a node to its right, while for a red node the interaction is to its left. (b) Hexagonal network with $n = 3$. The figure shows one of the possible interactions that is updated (with a double green arrow). (c) One-dimensional network with $n = 3$. (For interpretation of the references to colour in this figure legend, the reader is referred to the web version of this article.)

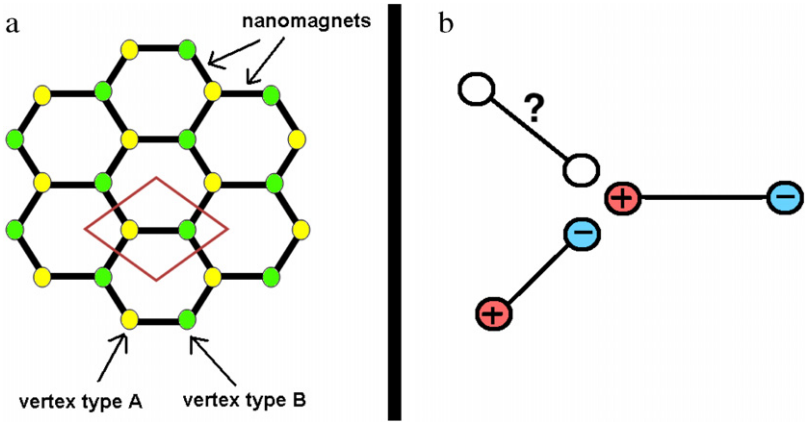

Fig. 2. (a) Scheme of the nanomagnet array. (b) Frustration in the hexagonal network.

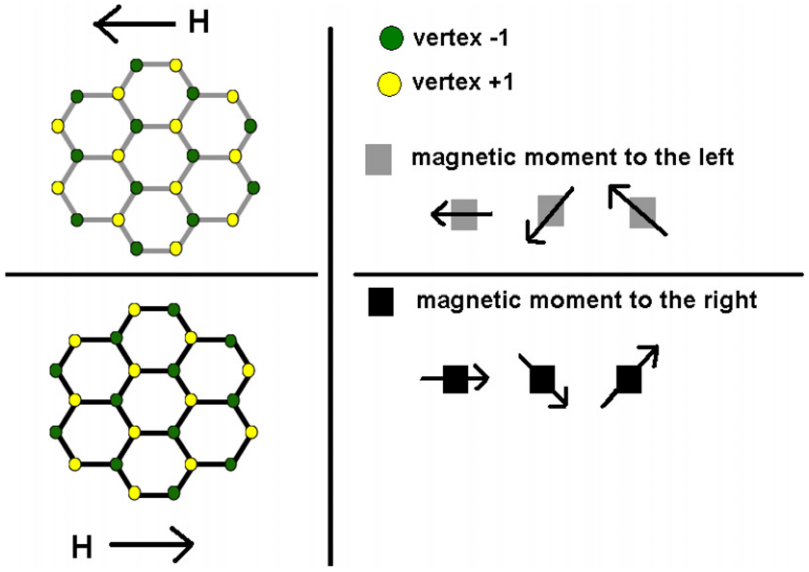

Fig. 3. Scheme of the nanomagnet array when the sample is totally saturated by the influence of an external magnetic field.

of Fig. 3). Under this condition, we define a positive and mobile monopole, if a nanomagnet converging in a class A vertex inverts its magnetic moment. The charge of vertex A goes from $q_A = -1 \rightarrow q_A^* = +1 \Longrightarrow \Delta q_A = +2$. If this is produced in a B type vertex, we define a negative monopole and would have $q_B = +1 \rightarrow q_B^* = -1 \Longrightarrow \Delta q_B = -2$, where q_A^* and q_B^* represent the charges of the vertex after the inversion and q_A and q_B represent the charges of the vertices A and B, respectively, in the their initial states. In this manner, when a nanomagnet inverts its magnetic moment, there emerges a monopole–antimonopole pair.

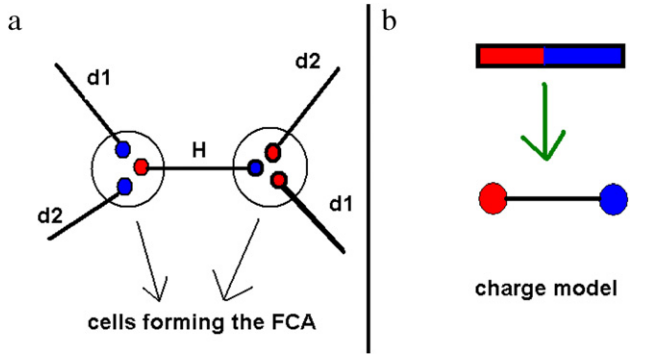

Fig. 4. (a) Scheme of the FCA cells. (b) Scheme of replacing the magnetic moments by the magnetic charge model.

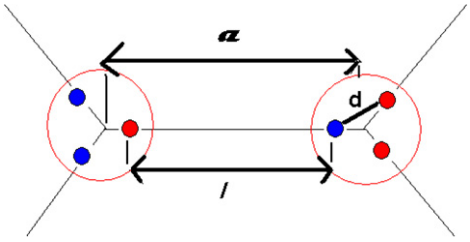

Fig. 5. Scheme of the configuration of charges in each vertex and of the length parameters.

If the three nanomagnets that converge in a vertex invert their moments, the condition $\Delta q_A = +2$ and $\Delta q_B = -2$ is also generated, but in this case the monopoles remain trapped and do not move through the sample.

The magnetic charge model

The moment $\overrightarrow{m}$ of each nanoisland in this model is replaced by two charges (one positive and the other negative), located at the ends of the nanomagnet, as shown in Fig. 4(b). The magnitude of each charge is $q = \frac{m}{l}$, where l is the length of the bar. The total charge in each vertex is the sum of the three charges associated with the vertex. Vertex j gives $Q_j = \sum_{k\epsilon j} q_k$ and the total energy of the system is given by the expression

$$U = \begin{cases} \frac{1}{2}\frac{\mu_0}{4\pi}\sum_{i,j}\frac{Q_i Q_j}{r_{ij}}, & i \neq j \\ f_i, & i = j. \end{cases} \tag{2}$$

The term for $i \neq j$ takes into account the interaction among the vertices of the array. The term $i = j$ considers the energy of the site. This term considers the interaction among the ends of the three nanomagnets that converge. Fig. 5 shows a scheme of the configuration of charges in each vertex and the parameters of the associated length.

The energy in each vertex is given by the expression

$$f_i = \frac{\mu_0}{4\pi}\left\{\frac{q_1 q_2}{d} + \frac{q_1 q_3}{d} + \frac{q_2 q_3}{d}\right\}. \tag{3}$$

In accordance with the parameters of the hexagonal lattice, $d = \frac{\sqrt{3}}{2}(a - l)$. Defining $q_0 = \frac{m}{l}$ and writing the energy in units of $\frac{\mu_0 q_0^2}{4\pi a}$, the total energy can be written as

$$U = \begin{cases} \frac{1}{2}\sum_{i,j}\frac{Q_i Q_j}{r_{ij}}, & i \neq j \\ \frac{2}{\sqrt{3}\varepsilon}\{q_1 q_2 + q_1 q_3 + q_2 q_3\}, & i = j. \end{cases} \tag{4}$$

Here $\varepsilon = 1 - \frac{l}{a}$. When the automaton is updated, the change in total energy is registered (using Eq. (4)), that is, under the magnetic charge model. The interaction of the charges with the applied magnetic field and the anisotropy energy are added to the total energy.

Reversal of the magnetization for a sample with very few impurities (system 1)

The system studied (system 1) is composed of 4600 nanomagnets, arranged in a region of 40 μm $\times$ 40 μm. The lattice constant has a value of 577 nm and the length of the nanoislands is 470 nm. The anisotropy energy is 56×10^4 K. The simulation contemplates a completely magnetized nanoisland array with the magnetic moment directed to the left. A magnetic field is applied to reverse the magnetization. The lower part of Fig. 6 shows the magnetic average polarization per nanoisland, the total density of magnetic monopoles (including mobile and non-mobile monopoles) and the density of the mobile monopoles (in units of total maximum density of the monopole $\sigma_{\max}$), as a function of the applied magnetic field (in oersteds), in the first phase of magnetic reversal. This system has 5% of the nanomagnets with the magnitude at the magnetic moment m_i in the range $0.99\, m \leq m_i \leq m$, where m is the moment when 95% of the nanoislands remain.

These results show that magnetic reversal begins at the extreme left and right of the sample. North–south monopole pairs are generated in these extremes, but only one of them is mobile, while the other remains trapped in the end and does not contribute to the mobile density. Fig. 6 (upper part) shows a scheme for different field values in the magnetic reversal of this system. It can be seen clearly in Fig. 6 that the northern monopoles (red circles) are moving to the right and the southern monopoles (blue circles) are moving to the left in response to the applied magnetic field. Also, the Dirac string associated with the magnetic monopoles can be clearly seen. When the northern and southern fronts meet they are annihilated as the Dirac strings are joined. Only trapped monopoles (and not mobile monopoles) participate in the final reversal process. This behavior can be seen from analysis of Fig. 6 (lower part). Considering the graph of the density of the mobile monopoles of Fig. 6, we can appreciate that the maximum density of the mobile monopoles occurs at a magnetic field close to the coercivity value (127 Oe) and the total density presents a small plateau near to this value.

Magnetization reversal for a sample with impurities (system 2)

System 2 has all the parameters of system 1, but with 10% of the nanomagnets with the magnitude at the magnetic moment m_i in the range $0.9m \leq m_i \leq m$, where m is the moment when 90% of the nanoislands remain. The procedure for reversing magnetization is the same as that used for the previous system. The study of the magnetic average polarization per nanoisland and of the monopole densities is shown in Fig. 7. In contrast to the case for the study of system 1, the results of this simulation are in qualitative agreement with the experimental results of the study by Mengotti et al. [8]. The maximum density value of the emergent monopoles is close to 10%, which corresponds to the data reported in the study [8]. The magnetic polarization curve presents the same structure as the experimental data. However, the experimental system of Mengotti et al. studied a central region of the sample (without considering the edges in the statistics); the results are similar to those of our study (which considers the edges in the statistics). Consequently, we can conclude that there is little disorder in the experimental sample.

Fig. 7 (upper part) shows part of the magnetic reversal sequence for system 2. We can appreciate that owing to impurities the monopoles emerge randomly in the nanoisland array and not just at the ends, as in the first case. The emergent monopoles, which

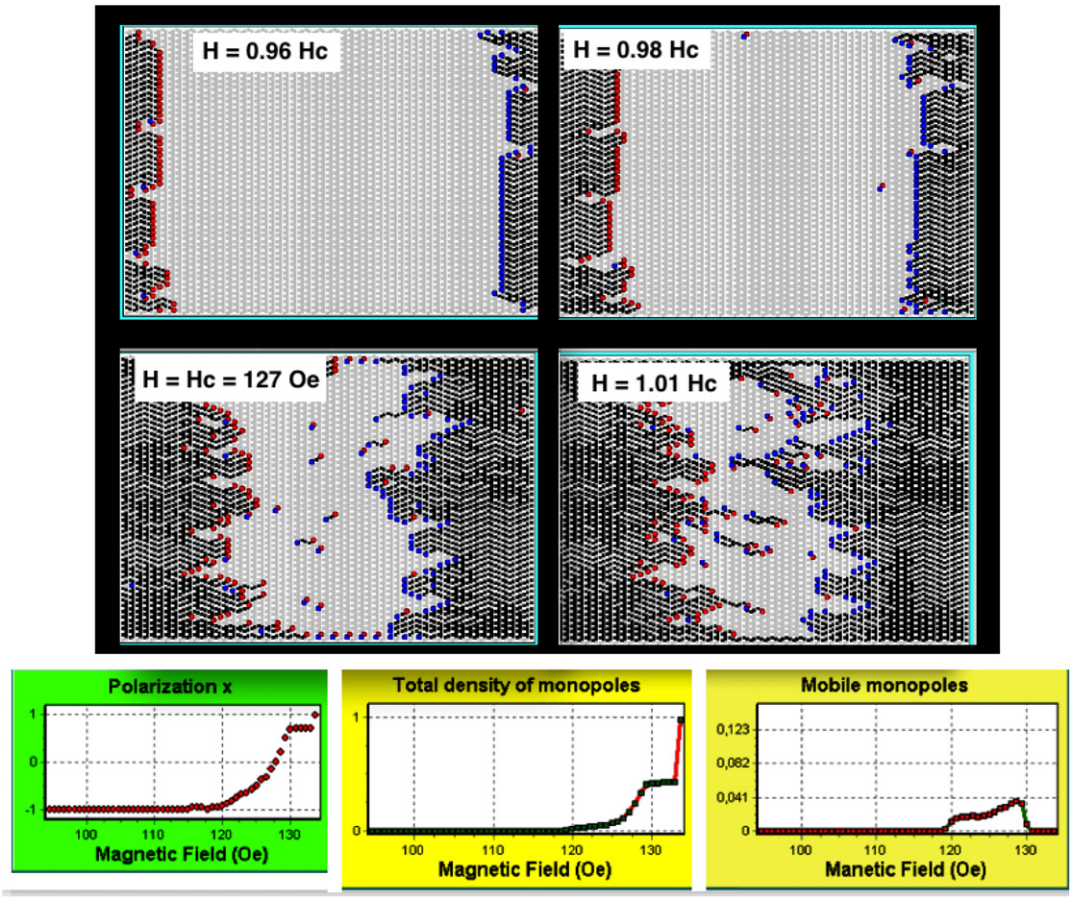

Fig. 6. Scheme of the four steps of the magnetic reversal simulation of system 1 using the FCA (upper part of the figure). The lower part of the figure shows the magnetic average polarization per nanoisland, the total density of magnetic monopoles (including mobile and non-mobile monopoles) and the density of the mobile monopoles (in units of the total maximum density of the monopole $\sigma_{\max}$), as a function of the applied magnetic field (in oersteds), in the first phase of magnetic reversal.

come from impurities and are generated in the central part of the nanomagnet arrays, move toward the ends, thus extending the Dirac string. This behavior is also well documented in the experimental results [8]. Considering graph of the density of the mobile monopoles of the Fig. 7, we can appreciate that the maximum density of the mobile monopoles occurs at a magnetic field close to the coercivity value (123 Oe) and the total density presents a small plateau near to this value.

Magnetic reversal in a square lattice

We now examine the behavior of the FCA model in the reversal of the lattice square of nanomagnets. This lattice is shown in Fig. 1(a). The frustration happens due to the fact that the four nanoislands that they converge to on a vertex cannot minimize its total energy. The system studied is a square of 2320 nanoislands with a surface area of 22 μm $\times$ 22 μm. The lattice constant is 570 nm and the length of the nanoislands is 470 nm. The anisotropy energy is on the order of 10^4 K. The sample contains 1% of impurities randomly located, with a similar value to that described for the hexagonal network. The initial configuration of this system is 100% magnetized in the direction 45° of the axis x. This implies that all the nanoislands in a horizontal direction have rightward magnetic moments, while all the vertically directed nanoislands have upward magnetic moments. We apply a magnetic field in the direction of the diagonal (45°) in the following manner: $\overrightarrow{H} = -H_x\hat{i} - H_y\hat{j}$, in the which the components of the field increase over time. The FCA algorithm operates with a similar updating sequence for each time stage. The sequence ($n \to w \to s \to e$) updates the connections, advancing counterclockwise. Fig. 8 (left) shows the change in magnetization as the applied magnetic field increases. The right part of the figures shows the density of emergent monopoles. The monopoles emerge when a nanoisland is inverted in a vertex. This implies that the sum of the electrical charges for this vertex is $+2$ (positive monopole) or -2 (negative monopole). Analysis of Fig. 8 shows that the magnetic reversal occurs with the appearance of these monopoles and the associated Dirac strings.

Fig. 9 shows some stages in the magnetic reversal for this system. We can note that in the first phase of the reversal, the monopoles occur at the four ends and that although the sample has impurities, there are no events in the center of the sample. In the first phase of the magnetic reversal, the Dirac strings move diagonally and are separated by a lattice site. When the reversal of these strings is completed, chains begin to form in free sites, giving rise to the second maximum in the density curve. This could explain the two peaks that can be observed in Fig. 8. In this case, the maximum density of mobile monopoles is between 2% and 3% of the maximum monopole density.

Propagation of binary information through a molecular array

We tested the FCA model with a problem of a one-dimensional molecular array. A recent theoretical work [18] studied the dynamics of a molecular array with a graphane structure [19, 20]. The aim of the work was to demonstrate that there is a set of geometric parameters that allow for transmitting binary information through a molecular cable. These molecules present two oxido-reduction centers (quantum dots) and when the

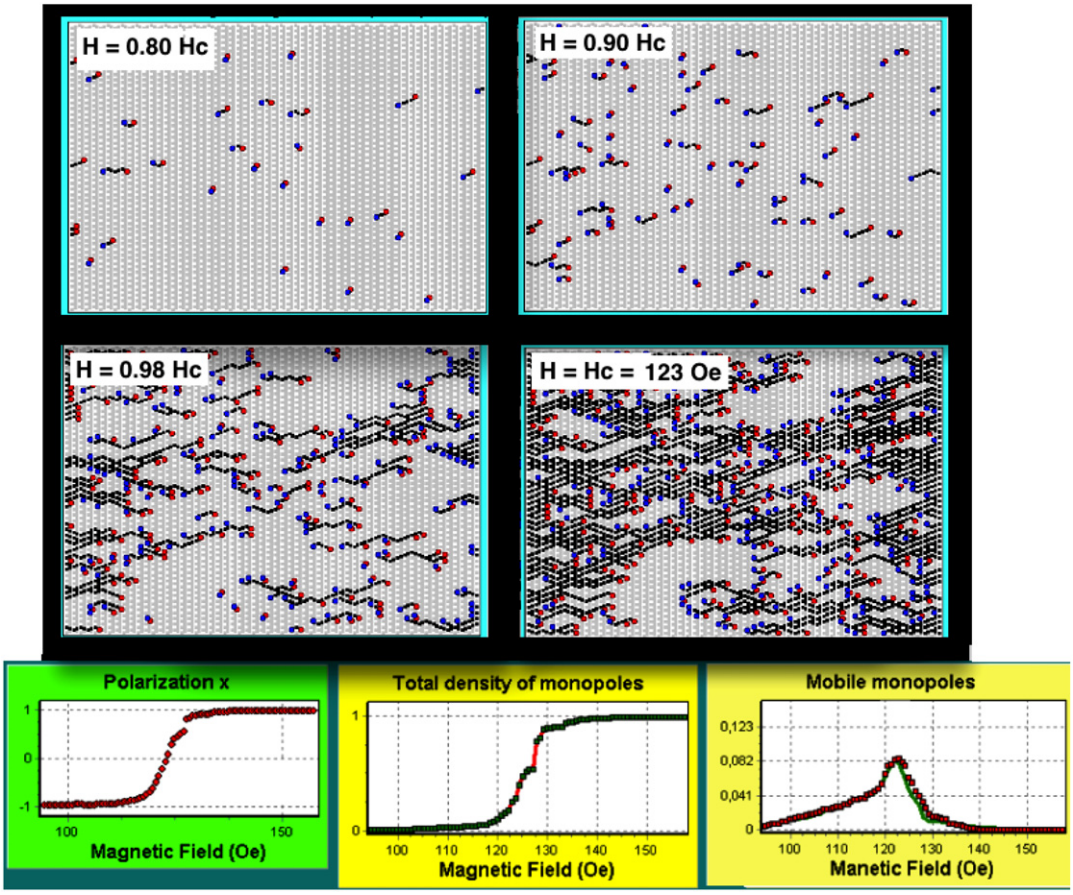

Fig. 7. Scheme of the four steps of the magnetic reversal simulation of system 2 using the FCA (upper part of the figure). The lower part of the figure shows the magnetic average polarization per nanoisland, the total density of magnetic monopoles (including mobile and non-mobile monopoles) and the density of the mobile monopoles (in units of total maximum density of the monopole σ_{max}), as a function of the applied magnetic field (in oersteds), in the first phase of magnetic reversal.

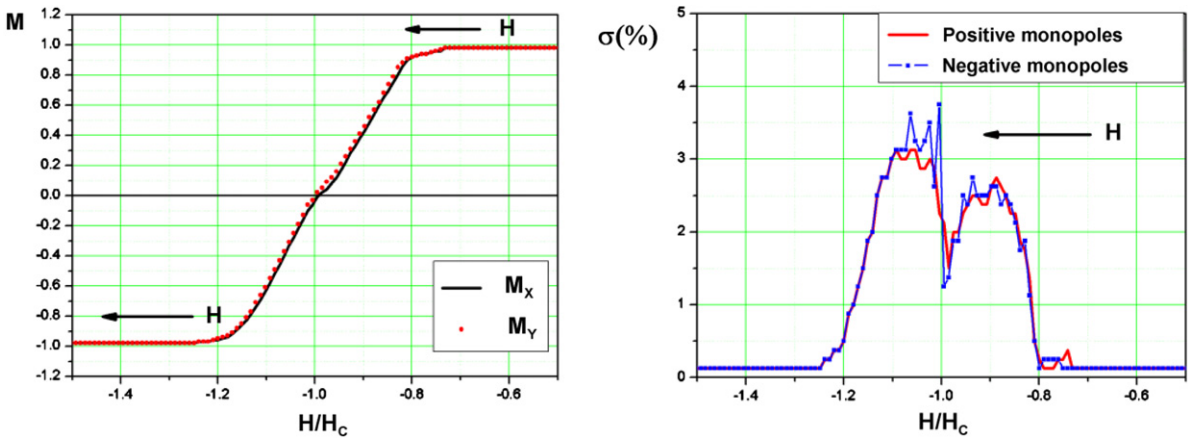

Fig. 8. The left part of the figure shows the average magnetization per nanoisland as a function of the applied magnetic field. The right part shows the density of monopoles (positive and negative) as a percentage of the density per site.

molecule is a cation, it presents a hole with a positive charge that can move between these quantum dots. The position of this charge excitation generates electrical polarization in the molecule. Depending on the position of the charge, the logic states 1 and 2 can be defined. Fig. 10 shows a scheme of the graphane type molecule and the proposed molecular array.

In the work with these structures [18], the distances that minimize the energy were studied and the value of the tunneling energy between quantum points was determined, all using first-principles calculations. The dynamic response of the molecular cable was studied with a model based on the Hubbard Hamiltonian. In this work we used the FCA model to determine the dynamic response of a cable formed by five molecules. The details of the units and parameters used are outlined in the work [18]. The polarization of the first molecule is manipulated externally and the changes in the polarization of the remaining four molecules are studied. The frustration in this array occurs because of an antiferromagnetic type of ordering occurring in order to minimize the

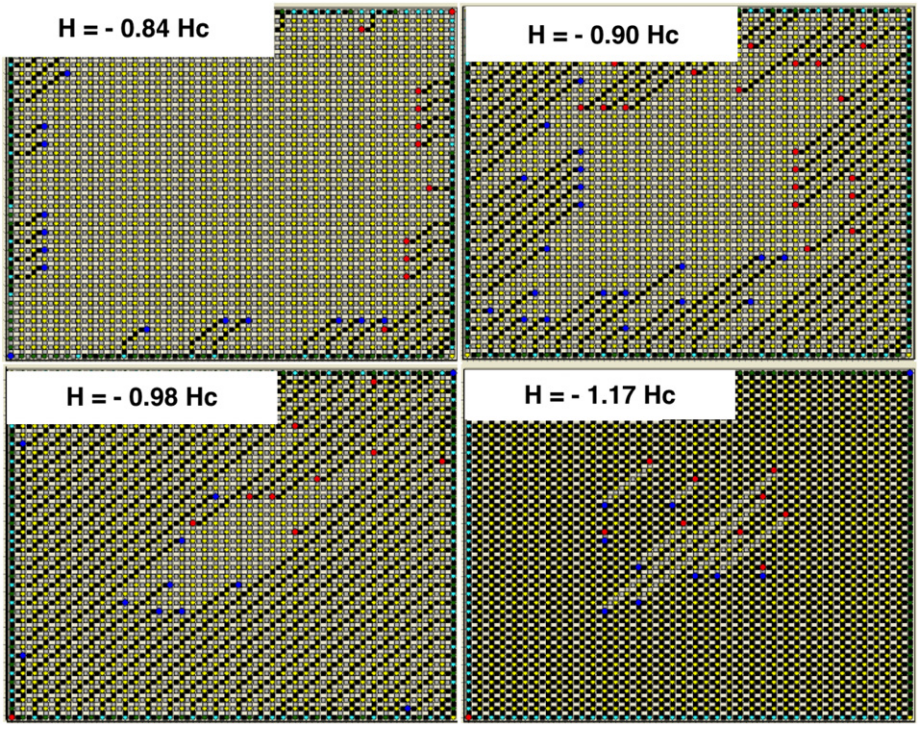

Fig. 9. Different steps of magnetic reversal of the lattice square studied. The gray squares indicate that the moments of the horizontal nanoislands are directed to the right and those of the vertical nanoislands are directed upward. The dark squares indicate the opposite directions in both cases. The red circles indicate positive monopoles. The blue circles represent negative monopoles. The yellow circles represent vertices with $q = 0$. (For interpretation of the references to colour in this figure legend, the reader is referred to the web version of this article.)

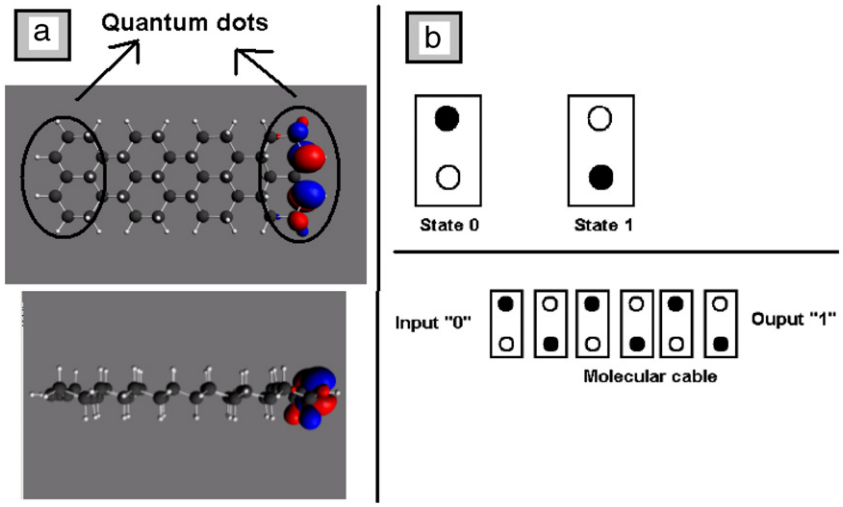

Fig. 10. (a) Scheme of the graphane type molecules. The large gray circles represent carbon atoms. The small circles represent hydrogen atoms. Also, part (a) represents the isosurface for the minimum energy state HOMO (with the charge at one of the quantum points). (b) The scheme of the logic states defined in the molecular cation and of an array of these molecules that define a molecular cable.

energy, during the reversal of the driver molecule. Therefore, we must actualize our automaton in two steps. The quantum component of the system is incorporated in the FCA algorithm with tunneling energy. Figs. 11 and 12 show the dynamics in the polarization of the five-molecule cable. In the first case (Fig. 11) an array of small molecules is studied. The distance between the quantum points is 6.6 Å and the tunneling energy is 1329 eV. The molecules are separated by a distance of 7.5 Å. The distances and the electrostatic energies involved imply that the thermal fluctuations are negligible. The second case, represented in Fig. 12, considers molecules where the distance between quantum points is 15.2 Å and the tunneling energy is 0.254 eV. We can appreciate that in the results for the first case, the first molecule does not succeed in polarizing the cable and the remaining four molecules remain in a state of permanent oscillation. In contrast, in the second case, the molecules change their polarization state in response to excitation. These results are in close agreement with the results shown for the same systems using the time-dependent Schrödinger equation [18]. This result is very important given that in studying more sophisticated systems, such as logic gates and

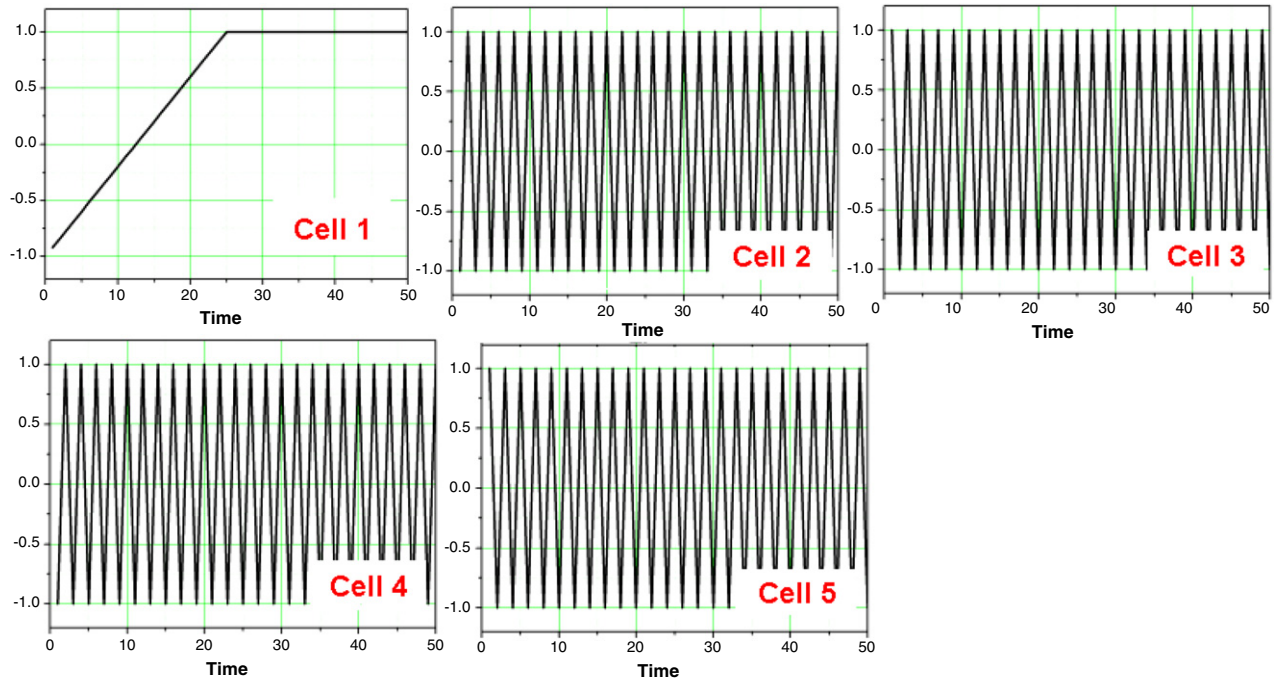

Fig. 11. Electrical polarization (in atomic units) of each molecule that forms the molecular cable for the small system explained in the text.

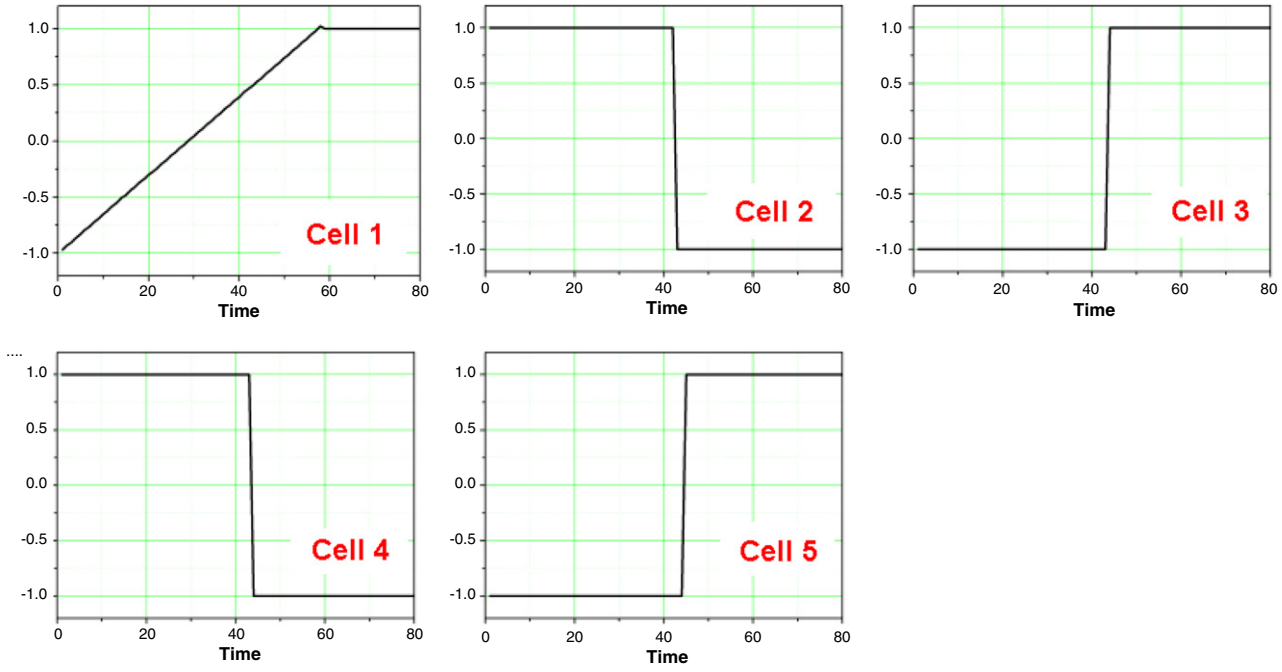

Fig. 12. Electrical polarization (in atomic units) of each molecule that forms the molecular cable for the large system explained in the text.

circuits, the Hamiltonian formalism of Hubbard cannot be applied to study the dynamic response.

Conclusion

This work presents a semi-deterministic model used to study frustrated systems. It is specifically designed for magnetic nanoisland arrays and charged molecules, but can be applied to any problem where there is frustration and where thermal fluctuations are negligible. The great advantage of the model is that it can make efficient simulations of highly complex phenomena in real time with a minimum of computational requirements. All the simulations shown in this paper were carried out using in a personal desktop computer [21]. They represent a perfect complement to the methods based on Monte Carlo algorithms for studying the elemental physics of problems with quantum entities.

Acknowledgment

The author acknowledge the financial support of FONDECYT program grant 11100045.

References

[1] V.F. Petrenko, R.W. Whitworth, Physics of Ice, Oxford Univ. Press, 1999.
[2] D.J.P. Morris, et al., Science 326 (2009) 411–414.

[3] T. Fennell, et al., Science 326 (2009) 415–417.
[4] H. Kadowaki, et al., J. Phys. Soc. Japan 78 (2009) 103706.
[5] R.F. Wang, et al., Nature 439 (2006) 303–306.
[6] E. Mengotti, et al., Phys. Rev. B 78 (2008) 144402.
[7] A. Remhof, et al., Phys. Rev. B 77 (2008) 134409.
[8] E. Mengotti, et al., Nat. Phys. 7 (2011) 68.
[9] A.O. Orlov, I. Amlani, G.H. Bernstein, C.S. Lent, G.L. Snider, Science 277 (1997) 928.
[10] J. Jiao, G.J. Long, F. Grandjean, A.M. Beatty, T.P. Fehlner, J. Am. Chem. Soc. 125 (2003) 7522.
[11] D. Griffeath, C. Moore (Eds.), New Constructions in Cellular Automata, University Press, Oxford, 2003.
[12] A. León, Z. Barticevic, M. Pacheco, Solid State Commun. 152 (2012) 41–44.
[13] G.Y. Vichniac, Physica D 10 (1984) 96.
[14] Y. Pomeau, J. Phys. A 17 (1984) L-415.
[15] H.J. Hermann, J. Stat. Phys. 45 (1986) 145.
[16] H. Ottavi, O. Parodi, Simulation of the Ising model by cellular automata, Europhys. Lett. 8 (1989) 741–746.
[17] J.H. Cole, C.L. Hollenberg, S. Prawer, Comput. Phys. Comm. 161 (2004) 14.
[18] A. León, M. Pacheco, Electronic and dynamics properties of a molecular wire of graphane nanoclusters, Phys. Lett. A 375 (2011) 4190–4197.
[19] J.O. Sofo, A.S. Chaudhari, G.D. Barber, Phys. Rev. B 75 (2007) 153401.
[20] D.C. Elias, et al., Science 323 (2009) 610.
[21] MacBook Pro, 2,7 GHz Intel Core i7.